Solar Energy 174 (2018) 386–398

Contents lists available at ScienceDirect

Solar Energy

journal homepage: www.elsevier.com/locate/solener

# Roadmap for the next-generation of hybrid photovoltaic-thermal solar energy collectors

A. Mellor[a,*], D. Alonso Alvarez[a], I. Guarracino[b], A. Ramos[b], A. Riverola Lacasta[c], L. Ferre Llin[d], A.J. Murrell[e], D.J. Paul[d], D. Chemisana[c], C.N. Markides[b], N.J. Ekins-Daukes[a]

[a] Department of Physics, Imperial College London, London SW7 2AZ, UK
[b] Clean Energy Processes (CEP) Laboratory, Department of Chemical Engineering, Imperial College London, London SW7 2AZ, UK
[c] Applied Physics Section of the Environmental Science Department, University of Lleida, c/Pere Cabrera s/n, 25001 Lleida, Spain
[d] School of Engineering, University of Glasgow, G12 8LT, UK
[e] Naked Energy Ltd, Unit 72, Basepoint Business Centre, RH11 7XX, UK

ARTICLE INFO

*Keywords:*
Hybrid photovoltaic-thermal
Pvt
Emissivity

ABSTRACT

For hybrid photovoltaic-thermal collectors to become competitive with other types of solar energy converters, they must offer high performance at fluid outlet temperatures above 60 °C, as is required for space heating and domestic hot water provision, which together account for nearly 50% of heat demand. A roadmap is presented of the technological advances required to achieve this goal. Strategies for reducing convective, radiative and electrical losses at elevated temperature are discussed, and an experimental characterisation of a novel transparent low-emissivity coating for photovoltaic solar cells is presented. An experimentally-validated simulation formalism is used to project the performance of different combinations of loss-reduction strategies implemented together. Finally, a techno-economic analysis is performed to predict the price points at which the hybrid technologies along the roadmap become competitive with non-hybrid photovoltaic and solar thermal technologies. The most advanced hybrid technology along the roadmap employs an evacuated cavity, a transparent low-emissivity coating, and silicon heterojunction photovoltaic cells.

## 1. Introduction

The growth of photovoltaic (PV) solar energy capacity worldwide has been hailed as a great leap forward in the battle to curb climate change, reduce dependence on finite fossil fuel reserves, and achieve energy independence for many nations. In the past decade, installed capacity has risen from 5.1 to 320 GWe (Philipps and Warmuth, 2017). Early growth has been stimulated by government subsidies; however, the more recent and substantial upturn has been driven by the ever-falling production costs of crystalline silicon (c-Si) PV modules. As a result, PV solar energy has now reached so-called grid parity in many parts of the world (Rocky-Mountain-Institute et al., 2014; Shah and Booream-Phelps, 2015; Shah et al., 2014), is soon expected to become one of the cheapest forms of energy supply (Green, 2016), and has been projected to represent 35% of global newly installed capacity by 2040 (Bloomberg-New-Energy-Finance, 2015).

As production costs fall and solar penetration becomes significant, we enter into a new era in which module costs are no longer the limiting factor to growth. The new challenges faced are numerous. Firstly, solar generation is intermittent and the daily and annual generation profile does not match demand, meaning that mass energy storage must be employed to enable increased penetration. Secondly, the cost of installation of a PV module is now greater than the production cost (Mayer et al., 2015), and the highest material cost is the encapsulation rather than the PV solar cells (Green, 2016). Thirdly, if solar generation is to be deployed in a distributed nature – close to the point of use – then the amount of suitable space for installations will become increasingly scarce, particularly in urban environments. In light of these considerations, it is believed that PV technologies will increasingly have to compete on overall power density (i.e. watts per unit area), and not only on the cost-per-watt of the module, which is presently the most commonly cited figure of merit (Green, 2016).

Conversely, solar thermal (ST) collectors have relatively high collection efficiencies up to 80%, (Solar-Rating-and-Certification-Corporation, 2007) low costs at around 1–8 €-ct/kWh (Mauthner et al., 2014), and are mature, with 435 $GW_{th}$ installed globally (REN21, 2016). Nonetheless, 'the annual rate of installed capacity is far less than for PV, largely since thermal energy is presently considered less

* Corresponding author.
*E-mail address:* amellor8@googlemail.com (A. Mellor).

https://doi.org/10.1016/j.solener.2018.09.004
Received 22 February 2018; Received in revised form 30 August 2018; Accepted 3 September 2018
Available online 20 September 2018

**Nomenclature**

*Abbreviations*

| | |
|---|---|
| PV | photovoltaic(s) |
| c-Si | crystalline silicon |
| PVT | photovoltaic-thermal |
| ST | solar thermal |
| CSP | concentrating solar power |
| IEA | International Energy Agency |
| ITO | indium tin oxide |
| NOCT | nominal operating cell temperature |
| DHW | domestic hot water |
| EVA | ethylene vinyl acetate |
| NIST | National Institute of Standards and Technology (U.S.) |
| MIR | mid-infrared |
| DMD | dielectric-metal-dielectric |
| TCO | transparent conductive oxide |
| CIGS | copper indium gallium selenide |
| Al-BSF | aluminium back surface field |
| PERC | passivated emitter rear contact |
| HJT | heterojunction technology |
| ARC | anti-reflection coating |
| PR | performance ratio |
| AR | annual revenue |
| FiT | feed in tariff |
| SPF | seasonal performance factor |
| PBP | payback period |

*Symbols: Relating to PV cells*

| | |
|---|---|
| $\eta$ | efficiency (%) |
| $T_{cell}$ | cell temperature (°C) |
| $\eta_{STC}$ | efficiency under standard test conditions (%) |
| $\beta$ | temperature coefficient |

*Relating to PVT collectors*

| | |
|---|---|
| $\eta_{th}$ | thermal efficiency (%) |
| $\eta_{opt}$ | optical efficiency (%) |
| $a$ | linear heat loss coefficient ($W\,m^{-2}\,°C^{-1}$) |
| $T_m$ | mean fluid temperature (°C) |
| $T_a$ | ambient temperature (°C) |
| $\varepsilon$ | emissivity (dimensionless) |
| $\alpha$ | absorptivity (dimensionless) |

*Relating to the techno-economic analysis (Subscripts denote electrical (el) or thermal (th) outputs. Superscripts denote PV, PVT or ST collectors. e.g. $Y_{el}^{PVT}$ is the annual electrical energy yield of a PVT collector)*

| | |
|---|---|
| $Y$ | annual energy yield ($kWh\,m^{-2}\,year^{-1}$) |
| $\eta$ | collector efficiency (%) |
| PR | performance ratio (%) |
| $H$ | annual insolation ($kWh\,m^{-2}\,year^{-1}$) |
| $T_d$ | fluid delivery temperature (°C) |
| $p$ | price at which energy is sold or price of energy displaced ($) |
| $AR$ | annual revenue generated from energy output ($\$\,m^{-2}\,year^{-1}$) |
| $CS$ | carbon savings from total energy output ($kgCO_2\,m^{-2}\,year^{-1}$) |
| $CI$ | carbon intensity of displaced energy ($kgCO_2$/kWh) |
| $SPF$ | seasonal performance factor of heat pump (dimensionless) |
| $PBP$ | payback period (years) |
| $C$ | total system cost including collector, rest of system and installation ($) |

valuable than electricity, is more difficult to transport without losses and new infrastructure, and is less versatile. However, a great advantage of thermal energy that will become of increasing importance is that it can be stored more efficiently and cheaply than electricity (Branz et al., 2015). Moreover, nearly half of the energy consumed globally is finally used as heat (International-Energy-Agency, 2012), generated either using gas, electricity, oil, biomass or other sources. Using distributed ST collectors equipped with thermal storage to displace electricity demand for heat generation is therefore a viable means of increasing solar penetration whilst dealing with intermittency of the solar resource. Solar heat therefore holds a great deal of untapped potential.

Within a high-penetration landscape, many benefits are offered by hybrid photovoltaic-thermal (PVT) collectors, which generate both electricity and thermal energy from a single aperture area (Zondag, 2008). These have a similar electrical efficiency to purely PV modules (Good et al., 2015), but with an added thermal efficiency of up to 60% (under low temperature operation) (Zondag, 2008). It has already been pointed out that employing concentrating PVT in centralized power plants can help address the storage challenge, whilst maximising the economic value of the energy produced per unit installation area, as compared to purely PV or concentrating solar power (CSP) power plants (Branz et al., 2015). However, considering that nearly half of the energy consumed globally is finally used as heat (International-Energy-Agency, 2012), it is clear there is also a significant opportunity to deploy distributed PVT collectors on residential, industrial and commercial sites, and to store and use the generated thermal energy to directly satisfy the local heat demand, whilst using the electricity either on-site or distributing via the grid.

In spite of the above considerations, the uptake of PVT has so-far been extremely modest. The installed capacity is presently too low to be reported, although a number of commercial products have appeared on the market (Good et al., 2015; International-Energy-Agency, 2008). Cited barriers to growth include product immaturity, a lack of specific standards (Good et al., 2015) (although these have been recently introduced (Network, 2015)), and reliability concerns over collector longevity due to daily thermal cycles, which is a topic of ongoing research (Magalhães et al., 2016).

A more fundamental barrier is the often-cited dilemma faced by PVT technology: both the electrical and thermal efficiency decrease with the PV-cell temperature, whereas the utility of the delivered thermal energy increases with this temperature. The majority of PVT systems deployed to date have aimed at delivering low temperature heat ($< 40\,°C$). Unglazed panels, which have particularly high heat losses, are often favoured for these low-temperature applications, since they keep the PV cells cooler, and so improve electrical efficiency. However, a low-temperature thermal output is able to satisfy relatively few end-use demands, e.g. swimming pool heating, which represent a tiny proportion of global heat demand; thus reducing the market potential of PVT as compared to purely PV or solar-thermal collectors.

PVT technology would achieve a significantly greater market potential if it were optimised to deliver thermal energy at temperatures of 40–60 °C. These temperatures are sufficient for domestic hot water (DHW) and space heating. As an example, roughly 50% of U.S heat demand requires temperatures in this range (Fox et al., 2011), corresponding to around 20% of total U.S final energy use (Philibert, 2006). A more ambitious strategy would therefore be to optimise PVT collectors to deliver thermal energy at these higher temperatures, whilst mitigating thermal and electrical losses, and ensuring collector longevity. There are now glazed collectors on the market that go some way towards achieving this (ENERGIES-SOL, 2015; Solimpeks, 2016)).

However, there is significant scope for performance improvement through further innovation, as is shown in this work.

This work presents a roadmap of the technological advances that are required for PVT collectors to achieve competitive conversion efficiencies and payback times whilst delivering thermal energy at a useful temperature. For the first time, a systematic techno-economic analysis is made of the benefits of combining different permutations of evacuated cavities, transparent low-emissivity coatings, and emerging PV technologies with low temperature coefficients, within a single collector.

Section 1 presents an introduction to the temperature dependence of PVT performance, highlighting the issues faced. Section 2 lays out the roadmap and discusses the different loss-control measures that are available, including a novel indium tin oxide (ITO)-based transparent low-emissivity coating applied directly to a PV cell, presented here for the first time. Section 3 projects the performance enhancements of these technological advances, and Section 4 examines how these enhancements are likely to affect the revenue generation, carbon savings, and investment payback period of PVT systems as compared to PV and ST systems. Conclusions are given in Section 5.

## 2. Temperature-dependent losses in PVT collectors

A principle challenge faced by PVT technology is the often-cited temperature dilemma: both the electrical and thermal efficiency decrease with the PV-cell temperature, whereas the utility of the delivered thermal energy increases with this temperature. This is exemplified in Fig. 1(a), which shows typical thermal (solid blue) and electrical (solid red) efficiencies of today's PVT collectors. Details on the PVT collector for which data is shown are given in Section 3.

On the thermal side, PVT suffer severe losses with increasing temperature due to convective, radiative – and to a lesser extent conductive – heat loss. These losses are also present in purely solar thermal (ST) collectors. However, the best performing ST collectors employ heat-loss-minimization measures such as evacuated cavities and low-emissivity coatings that are absent from the present generation of PVT collectors, and so perform better at higher temperatures (black curve in Fig. 1).

On the electrical side, PV cells tend to reduce in efficiency with increasing temperature. This temperature dependence will, in principle, be the same for cells in a PVT collector as for the same cells in a purely PV module. However, the so-called nominal operating cell temperature (NOCT) in a PV module is around 50 °C in full sunshine (depending on local weather conditions and module design), whereas cells in a PVT collector will operate at or above the fluid delivery temperature, which for the larger market applications will be higher than 50 °C.

Shown in Fig. 1(b) are the temperature ranges for different heat demands that can be met by solar thermal or PVT collectors, along with the percentage of total U.S. heat demand that these represent; both the ranges and demand percentages have been estimated by Fox et al. (2011). The demand percentage for swimming pool heating, space heating and domestic hot water (DHW) represent real demand, whereas the given demand percentage for air conditioning represents a potential thermal demand if this service were provided by sorption cooling systems (Wang et al., 2009) instead of electrical cooling systems.

We focus on space heating and DHW as the principle market for PVT. In the case of the U.S., this represents a full 50% of heat demand (Fox et al., 2011), and therefore around 20% of total U.S final energy use (Philibert, 2006). Specific estimates for other countries are hard to come by; however, the fact that heat use makes up nearly 50% of final energy use, and that this is dominated by space heating and DHW is mirrored in Europe (Power, 2006), for example. Fox et al. determined a 40–60 °C temperature range for these services, based on U.S. Department of Energy recommendations. In this work, we choose the more conservative upper bound of this range (60 °C) as the required delivery temperature for space heating and DHW to allow for system losses and to make the results applicable to different geographical regions.

The circular markers denote the thermal (blue) and electrical (red) efficiencies of today's flat panel PVT collectors at 60 °C fluid outlet temperature. For this application, the thermal efficiency of today's PVT collectors are roughly half that of the best solar collectors (black circle) and the electrical efficiency around 3 percentage points lower than an equivalent purely PV module operating at NOCT (black cross). It is shown in Section 4 that this performance deficit makes it difficult for PVT to compete with either ST collector or PV modules at today's costs. The technical advances that are required to push PVT performance towards their target values and therefore improve competitivity are discussed in the following section.

## 3. Controlling losses in PVT collectors

Fig. 2(a) shows a simplified cross-section of a basic PVT collector. PV cells are mounted on a metal plate with an intermediate adhesive layer, which is thermally conductive but electrically insulating. A network of heat transfer pipes are welded to the rear of the plate to extract thermal energy to a water tank, and the plate and pipes are backed with an insulating material. The PV cells are encapsulated in ethylene vinyl acetate (EVA) and topped with a cover glass to prevent the cells being degraded from exposure to the moist ambient air. This type of collector is typically referred to as an unglazed collector, despite the presence of the PV cover glass, since there is no additional glazing layer. Thermal loses in this type of collector are dominated by convective and radiative losses from the top of the collector. Losses from the bottom and sides are small due to the rear insulation layer and the low aspect ratio,

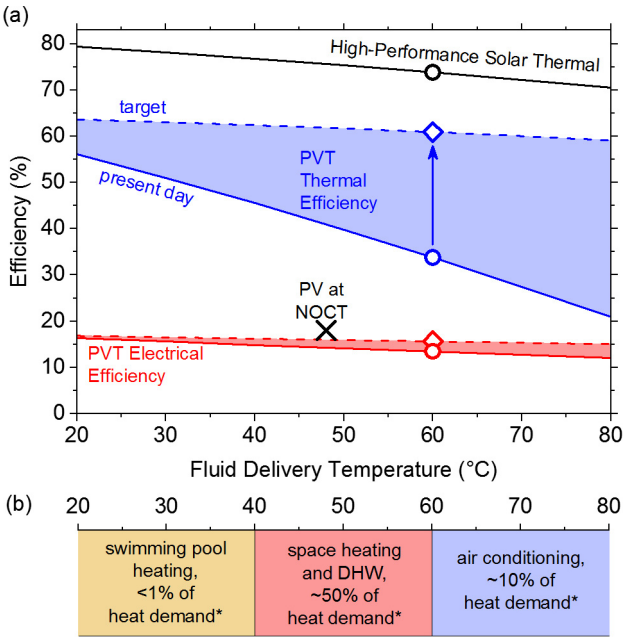


**Fig. 1.** (a) Solid curves: exemplary electrical (red) and thermal (blue) efficiencies of today's best commercially available PVT collectors (See Section 3 for details). Dashed curves: electrical and thermal efficiencies that can be achieved by implementing the technical advances laid out in this roadmap. Also shown for comparison is the thermal efficiency of a high-performance solar thermal collector (solid black curve), and the electrical efficiency of commercially available high-performance PV modules at their nominal operating cell temperature (NOCT) (black cross). All thermal efficiencies assume an irradiance of 1000 $Wm^{-2}$, an ambient temperature of 20 °C, and a wind speed of 0 $ms^{-1}$. (b) Temperature ranges at which delivered fluid is required for some different heat demands. Also shown is the percentage of total U.S. heat demand that these demands represent. Both ranges and demands are reproduced from Fox et al. (2011). (For interpretation of the references to colour in this figure legend, the reader is referred to the web version of this article.)

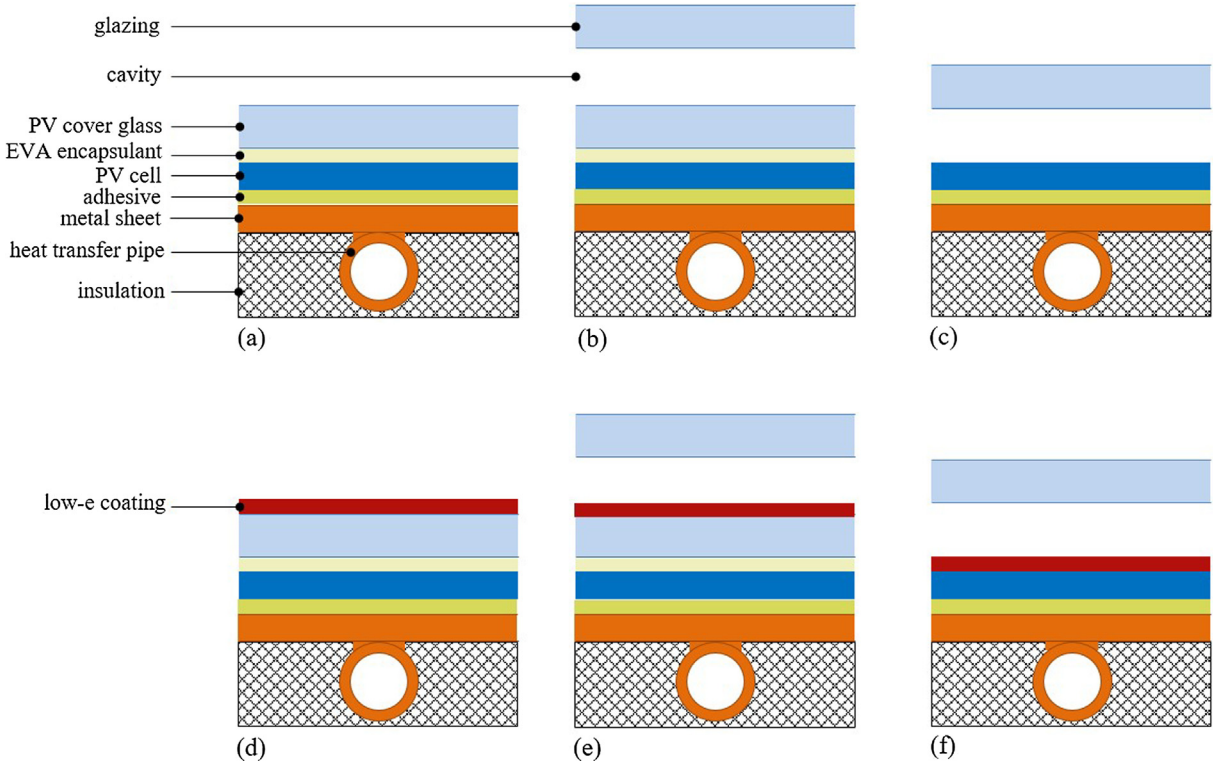


**Fig. 2.** Cross-section schematics PVT collectors with different heat-loss control mechanisms. (a): a so-called unglazed collector. (b): a glazed collector for reduced convective heat loss. (c): a glazed collector in which the PV cover glass and encapsulant has been removed for improved reliability during high-temperature operation (d)–(e): same as (a)–(c) but with an additional low-e coating to reduce radiative heat loss.

respectively. For a more detailed description of PVT collector design, see e.g. Zondag (2008).

### 3.1. Controlling convective losses

In ST technology, convective losses can be controlled by applying an additional glazing layer to create a cavity between the solar absorber and the ambient air (Bisen et al., 2011; Buchberg et al., 1976; Zondag, 2008). This cavity is typically filled with air, but can also be filled with an inert gas, such as argon, for improved insulation (Vestlund et al., 2012; Vestlund et al., 2009). One step further is to suspend the absorber in an evacuated tube, which all but supresses convective losses; however, this comes at the cost of reducing the packing density of the absorber, and hence reducing the so-called optical efficiency (i.e. the fraction of incident sunlight that is absorbed). The choice between evacuated tube and so-called flat plate glazed collectors depends on the geographical location and desired temperature of fluid delivery. In 2014, unglazed collectors, glazed collectors and evacuated tube collectors accounted for 6%, 22% and 71% of global solar-thermal capacity, respectively. The market therefore typically favours convective-loss control at the expense of lower optical efficiency. More recently, a flat-plate-evacuated ST collector has appeared on the market (TVP-Solar), which promises the combination of high optical efficiency and minimal convective thermal loss.

PVT collectors are presently less advanced in the progression from unglazed to glazed to evacuated designs, compared to ST collectors. Whilst many unglazed and glazed designs have been developed by research groups (Zondag, 2008), most commercial PVT collectors installed today are unglazed (Strategy, 2016). Nonetheless, more glazed collectors have appeared on the market in recent years (Solimpeks), and there is now an evacuated-tube PVT collector at product development stage (Naked-Energy).

A schematic of a glazed PVT collector is shown in Fig. 2(b), where the cavity could in principle be filled with air, argon, or a vacuum. For a quick comparison between the thermal insulation offered by these strategies, we present in Table 1 estimates of the total heat transfer coefficient between the PV cells and the ambient air for unglazed and glazed PVT collectors containing various gases. These values are calculated using the formulae, material properties, collector geometry, inclination and wind speed given in Guarracino et al. (2016). The wind speed was 0 $ms^{-1}$. The relevant thermal properties of Air and Argon are taken from Chen and Saxena (1975) and the NIST database, respectively. The vacuum filled cavity admit a conductive heat transfer coefficient of 0.86 $Wm^{-2}K^{-1}$ due to the presence of conductive spacer pins (Henshall and Eames, 2014). The values shown consider only conductive and convective heat transfer. Rigorous calculations including parallel radiative heat transfer and rear losses are performed further on.

**Table 1**
The aggregate convective/conductive heat transfer coefficient through a glazing cavity containing different gases. These are calculated using the methodology and material properties given in Ref. (Guarracino et al., 2016). The gas properties used to calculate the coefficients are also shown.

| Glazing type | Cavity gas | Thermal conductivity/$Wm^{-2}K^{-1}$ | Dynamic viscosity/$Ns\,m^{-1}$ | Prandtl number | Convective/conductive heat transfer coefficient/$Wm^{-2}K^{-1}$ |
|---|---|---|---|---|---|
| Unglazed | – | – | – | – | 10.8 |
| Glazed | Air | 0.0275 | $1.63 \times 10^{-5}$ | 0.714 | 2.1 |
| Glazed | Argon | 0.0198 | $2.33 \times 10^{-5}$ | 0.614 | 1.7 |
| Glazed | Vacuum | 0 | – | – | 0.86 |

### 3.2. Removing EVA encapsulant and cover glass for improved PVT reliability

Like ST collectors, PVT collectors undergo so-called stagnation at certain times of the year when the thermal storage is fully loaded. Under stagnation condition, glazed collectors may reach temperatures up to 130 °C (Zondag and Van Helden, 2002), although higher temperatures would be expected for collectors with low-e coatings and argon-filled or evacuated cavities. At temperatures of 130 °C, and above, deterioration of the EVA encapsulant may occur, causing the PVT electrical efficiency to degrade more quickly than would be expected for a PV module, which does not experience such high temperatures (Zondag, 2008).

One possibility to remove this degradation mechanism is to remove entirely the EVA and cover glass, as shown in Fig. 2(c). The feasibility of encapsulant-free PV has been demonstrated recently in modules in which the cells are exposed to dry air (Mittag, 2017). This concept could therefore be transferred to glazed PVT collectors in which the cavity is free of moisture (e.g. if it contains dry air, argon or is evacuated).

### 3.3. Controlling radiative losses

Hot objects emit mid-infrared (MIR) radiation into the surroundings. This is significant loss mechanism in both ST and PVT collectors. In both unglazed and glazed PVT collectors (Fig. 2(a) and (b)), the principle radiative loss emanates from the PV cells, PV encapsulant and PV cover glass. In the configuration in Fig. 2(c), radiative loss is dominated by emission from the bare PV cells. Note that the upper glazing layer is closer to the ambient temperature and so radiation from this surface is less important.

The absorptivity/emissivity spectra of an unencapsulated silicon solar cell and of an encapsulated silicon solar cell with cover glass have been studied in detail by Riverola et al. (2018), and are both reproduced in Fig. 3. Note that the spectral absorptivity and emissivity of a body are nearly equal close to thermal equilibrium, and so only one curve is shown, which represents both quantities. Also shown are the irradiant intensity of the terrestrial solar spectrum (AM1.5G standard) and the radiative emission of a so-called black-body at 60 °C; both refer to the right axis. The overall absorption, $\alpha$, is the normalized convolution of the absorptivity/emissivity curve with the solar spectrum, and the overall emission, $\varepsilon$, is the normalized convolution of the absorptivity/emissivity curve with the black-body spectrum. $\varepsilon$ is shown for each curve in the label.

Both encapsulated and unencapsulated cells exhibit high MIR emissivities. This makes a significant contribution to the heat loss in today's PVT collectors (Zondag, 2008), and is partly responsible for their lower efficiencies compared to ST collectors. ST collectors control this loss by using spectrally selective low-emissivity (low-e) absorber layers, typically using black chrome (McDonald, 1975), black nickel (Cathro, 1975), copper oxide or metal-dielectric cermets (Zhang and Mills, 1992), which exhibit strong absorptivity (~90%) at solar wavelengths, but low emissivity (~10%) in the MIR. Radiative losses in PVT collectors can be suppressed using low-e coatings, located as shown in Fig. 2(d)–(f). These must be reflective in the MIR to trap emission in the collector, but transmissive at solar wavelengths to allow the underlying PV cells to generate electrical power. The absorptive low-e materials used in ST collectors are not, therefore, applicable. Instead dielectric-metal-dielectric (DMD) layer stacks or transparent conductive oxides (TCOs) can be used as transmissive low-e coatings as routinely used on automotive windscreens and energy efficient glazing (Hamberg and Granqvist, 1986; Solieman and Aegerter, 2006). Both types of coating have recently been investigated for PVT applications.

Lämmle et al. developed a low-e coating based on a thin silver film between dielectrics, and applied this to the cover glass atop the PV cells (as in Fig. 2(d)–(e)) (Lämmle et al., 2016). The spectral emissivity of the coated ensemble is reproduced in Fig. 3; it can be seen that the coating reduces the emissivity from 0.9 to 0.13, which is close to that of the best ST collectors. Lämmle et al. (2016) reported that the presence of the coating reduces the electrical efficiency of the PV output by 0.3 percentage points due to reduced solar transmission.

Our own research group has developed a low-e coating based on $In_2O_3$:Sn (ITO), and applied this to bare silicon PV cells (as in Fig. 2(f)). The spectral emissivity of the coated cells is shown in Fig. 3. The deposition process is described in Mellor et al. (2016), but the experimental absorptivity/emissivity spectrum is presented here for the first time. We also report a reduction of the electrical efficiency of the PV cell by 0.5 percentage points (a relative drop of 3%) due to transmission losses, although this can be reduced by further optimising the ITO layer thickness (Alonso-Álvarez et al., 2017a,b).

It can be seen that the DMD coating applied to the cover glass by Lämmle et al.[41] achieves significantly lower emissivity than the ITO coating applied to the bare silicon solar cell. This is in part due to the film itself, but in part due to the topology of the underlying surface; the silicon solar cell has a pyramidal surface texture, whereas the cover glass is planar. It is known that surface textures lead to increased emissivity (Riverola et al., 2018), and it has been shown that the same ITO coating applied to a planar silicon wafer leads to an emissivity of around $\varepsilon = 0.2$ (Alonso-Álvarez et al., 2017a,b), which is lower than when applied to a textured cell ($\varepsilon = 0.5$), but still higher than the $\varepsilon = 0.13$ achieved by the DMD coating on glass.

As described in Section 3.2 EVA-free PV has better reliability at high operating temperatures (in the case of glazed collectors with moisture free cavities). It is therefore desirable to achieve the same low emissivity in an EVA-free (Fig. 2(e)), as is possible in a collector with EVA and cover glass (Fig. 2(f)). This requires both an improvement in the coating (either a switch to DMD or an improved TCO solution), but could also be assisted by using planar PV cell types, such as CIGS, CdTe or un-textured silicon with multiple anti-reflective layers.

### 3.4. PV electrical efficiency loss

The sunlight to electrical power efficiency, $\eta_{el}$, of a PV solar cell

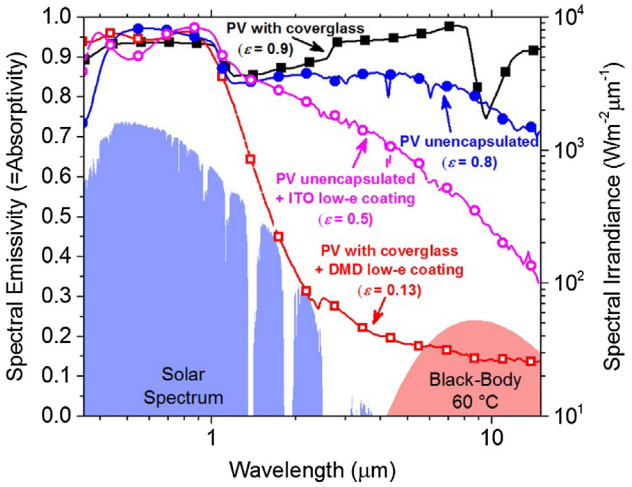


**Fig. 3.** Left axis: Experimental absorptivity/emissivity spectra of solar cells with and without low-e coatings. Black closed square markers: PV cells with EVA encapsulant and cover glass without low-e coating. Red open square markers: PV with encapsulant and coverglass with DMD low-e coating atop the coverglass. Blue solid circular markers: Unencapsulated PV without low-e coating. Magenta open circular markers: Unencapsulated PV cells with ITO low-e coating. Right axis: the Am1.5G solar spectrum (blue filled) and the Planck radiation spectrum of a black body at 60 °C (red filled). (For interpretation of the references to colour in this figure legend, the reader is referred to the web version of this article.)

decreases with the cell temperature, $T_{cell}$ and is well described (Dupré et al., 2015) by

$$\eta_{el}(T_{cell}) = \eta_{STC}(1-\beta(T_{cell}-25\,^{\circ}\mathrm{C})) \quad (1)$$

where $\eta_{STC}$ is the PV cell efficiency at standard test conditions (STC), i.e. $T_{cell} = 25\,^{\circ}\mathrm{C}$, and $\beta$ is the so-called temperature coefficient. Both parameters depend strongly on the type of PV cells being used.

In this work, we focus on different types of crystalline silicon solar cell, since this technology is likely to dominate the market in the coming years and possibly decades (ITRPV, 2017). Fig. 4 shows the temperature dependent efficiency of a number of commercial monocrystalline solar cells with different architectures. The parameters $\eta_{STC}$ and $\beta$ for each cell are taken from the product datasheets and are shown in Table 2 along with the source of the data. It should be observed that this data is exemplary, and that there is also some variation between different products with the same architecture. The aluminium back surface field (Al-BSF) architecture has dominated the market for some decades, but is beginning to be replaced by the passivated emitter rear cell (PERC), which typically offers a higher $\eta_{STC}$ but similar $\beta$. Perhaps of more interest for PVT is the newly emerging heterojunction (HJT) solar cell, which offers similar $\eta_{STC}$ to a PERC cell, but a significantly lower temperature coefficient.

If a PVT collector is delivering hot water at 60 °C, then $T_{cell}$ is likely to be around 70 °C. This is significantly higher than the nominal operating cell temperature (NOCT) of a PV module, which is typically 48 °C. The temperature coefficient is therefore of particular importance for PVT collector performance. In light of this, it may be beneficial for PVT developers to consider heterojunction solar cells in the next generation of collectors.

## 4. Performance comparison of PVT collector designs

In this section, we compare the projected performance of different PVT collector designs, using an experimentally validated PVT collector simulation methodology presented by Guarracino et al. (2016). We focus in particular on different permutations of the loss-control mechanisms described in the previous section. Regarding convection control, we consider glazed collectors in which the cavity contains air, argon, or a vacuum. Unglazed collectors are not considered, since these are a step below the present commercial state of the art. Regarding emissivity control we consider overall radiative emissivities of $\varepsilon = 0.9$, 0.5 and 0.15. The value of $\varepsilon = 0.9$ corresponds to no low-e coating; $\varepsilon = 0.5$ and 0.15 correspond to the low-e coatings discussed in Section 3.3. Regarding electrical efficiency, we consider PVT collectors incorporating the PERC and HJT silicon solar cells with parameters given in Table 2. These different designs constitute a roadmap for PVT technology development.

For all designs, the collector is a flat-plate collector with a gross area of $1.66 \times 0.86\,\mathrm{m}^2$, an absorber area of 98% of the gross area, and with 14 evenly spaced copper pipes on the rear. The fluid flow rate through the pipes is 62 L/hr. The geometry, materials and dimensions are described in detail in Guarracino et al. (2016), along with the experimental validation of the simulation methodology for this type of collector. These collector dimensions follow largely the commercially available Volther Powertherm PVT module (Solimpeks, 2017). The thermal calculation is performed assuming the PV cells are operating at maximum power point (MPP mode), and so extracting part of the incident irradiation as electrical power. This is appropriate since synchronous electrical and thermal generation is considered throughout this work. All calculations assume an ambient air temperature of 20 °C, a solar irradiance of $1000\,\mathrm{Wm}^{-2}$, and a wind speed is $0\,\mathrm{ms}^{-1}$. It should be observed that the thermal efficiency of PVT and ST collectors is not independent of irradiance. This is accounted for further on in Section 5.

The optical efficiency for the PVT collectors, i.e. the percentage of incident sunlight that is absorbed in the absorber region, varies significantly between different collectors (Al-Shamani et al., 2014). The highest optical efficiencies reported in literature are around $\eta_{opt} = 81\%$ (Al-Shamani et al., 2014; Antonanzas et al., 2015), and so we take this value as a realistic target for PVT. The value $\eta_{opt} = 81\%$ roughly breaks down into 8% reflection loss due to the glazing layer, which is reasonable if there is an anti-reflection coating (ARC) on both faces; 9% reflection loss at the surface of the PV cell or PV cover glass, which is an appropriate value when considering the entire solar spectrum (Santbergen and van Zolingen, 2008); and 2% loss due to the difference in total area and absorber area. In the case of evacuated collectors, we consider only flat plate designs (TVP-Solar), and so the optical efficiency is the same as for the other glazed collectors. Note that this optical efficiency is an input parameter to the calculations, and is distinct from the calculated zero-loss efficiency, $\eta_0$, discussed further on.

PV panels typically have efficiencies around 2 percentage points lower than the efficiency of the PV cells they employ. This is due to spaces between the cells, and some increased electrical losses when connecting cells into strings. Thus, PV panels employing the PERC and HJT cells shown in Table 2 will have module level efficiencies on the order of $\eta_{STC} = 19\%$. In a glazed PVT collector, similar losses may be expected, plus an additional relative 8% loss due to reflection from the additional glazing layer. The PVT electrical efficiency at $T_{cell} = 25\,^{\circ}\mathrm{C}$ is therefore taken to be $\eta_{STC} = 17.5\%$ for all collectors. The temperature coefficient, $\beta$, is taken to be the same as in Table 2, i.e., $-0.4$ and $-0.2\%/\mathrm{K}$ for PERC and HJT respectively.

Fig. 5(a) shows the projected thermal efficiency from each type of PVT collector, as a function of the fluid delivery temperature. The fluid delivery temperature is chosen as the $x$ ordinate since this determines what type of thermal demands can ultimately be supplied by the collector. The efficiency curves are grouped in terms of the convective and radiative loss controls they employ. It should be observed that the PV-cell temperature coefficient also affects the thermal efficiency. However, to simplify the plot, thermal efficiency curves are shown only for $\beta = 0.2\%/\mathrm{K}$, and we note that the thermal efficiencies would be higher by 1–2 percentage points if using PV cells with $\beta = 0.4\%/\mathrm{K}$. Also shown for comparison is the thermal efficiency of a flat-plate evacuated solar thermal collector with a well optimized low-e absorber ($\alpha = 0.9$, $\varepsilon = 0.1$). This represents the highest performing benchmark on the thermal side.

The glazed, air-filled PVT collector with $\varepsilon = 0.9$ is taken to represent the present commercial state-of-the-art. The projected thermal efficiency of this collector (solid black curve, square markers) are comparable to the values found in manufacturers' datasheets (Eurofins). It can be seen in Fig. 5 that significant thermal

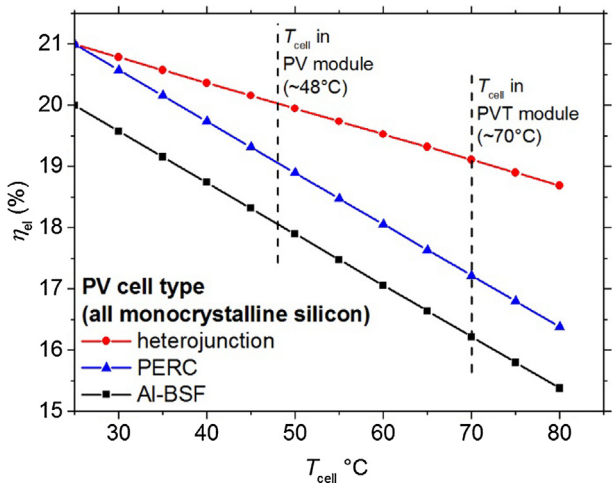


**Fig. 4.** Typical electrical efficiency of commercially available monocrystalline solar cells with selected architectures as a function of the cell temperature. Curves are produced using parameters from manufacturers' datasheets, which are listed in Table 2 along with sources.

**Table 2**
Solar cell performance parameters of commercially available monocrystalline solar cells with selected architectures. In each case, a specific solar cell product from a specific manufacturer is taken to represent the performance of the solar cell type, although it should be observed that there is variation between manufacturers and products, and cell performance is continually improving through product development.

| PV cell architecture | $\eta_{STC}$ (%) | $\beta$ (%/K) | Example manufacturer | Source |
|---|---|---|---|---|
| Al-BSF | 20 | −0.42 | Yingli Solar | (Yingli-Solar, 2017) |
| PERC | 21 | −0.40 | CSUN | (CSUN, 2017) |
| HJT | 21 | −0.20 | Meyer Burger | ((Meyer-Burger, 2017)) |

improvements can be expected from a combination of convection and emissivity control measures. The best performance is achieved by a flat-plate evacuated collector employing a low-e coating with $\varepsilon = 0.15$. However, marked improvements can also be observed for intermediate solutions, such as an argon filled collectors and evacuated tube collectors with $\varepsilon = 0.5$. These intermediate solutions may prove more interesting from a cost-benefit point of view, as is investigated in the following section.

As discussed previously, PVT collectors will need to deliver fluid at least 60 °C if they are to gain significant market share, since this temperature is required for space heating and DHW. At this temperature, the present PVT state-of-the-art achieves a thermal efficiency of around 35%, whereas an argon-filed collector with low-e achieves 50%, and an evacuated collector with low-e achieves 60%. This is to be compared to 75% efficiency for the high-performance ST collector at the same temperature. The difference between the best PVT collector and the ST collector is due to part of the solar irradiance being converted to more valuable electrical power in the PVT collector.

The thermal efficiency curves in Fig. 5(a) can be characterised by performing the following quadratic fit to obtain the zero-loss efficiency, $\eta_0$ (%), the first-order heat loss coefficient, $a_1$ ($Wm^{-2}K^{-1}$), and the second-order heat loss coefficients, $a_2$ ($Wm^{-2}K^{-2}$)

$$\eta_{th}(T_m) = \eta_0 - a_1\frac{T_m - T_a}{G} - a_2\frac{(T_m - T_a)^2}{G} \quad (2)$$

$T_m$, $T_a$ and $G$ are respectively the mean fluid temperature, the ambient temperature and the solar irradiance. Note that the fit is performed to the thermal efficiency curve with $T_m$ in the abscissa, and that the collector is in MPP mode as before.

**Table 3**
Zero-loss efficiency of PVT collectors with different combinations of glazing cavity filling (top row) and emissivity (left column).

| Zero-loss efficiency, $\eta_0$ (%) | $\varepsilon = 0.9$ | $\varepsilon = 0.5$ | $\varepsilon = 0.15$ | ST collector (Evacuated, $\varepsilon = 0.1$) |
|---|---|---|---|---|
| Air | 58 | 59 | 60 | 78 |
| Argon | 58 | 60 | 61 | |
| Evacuated | 59 | 60 | 62 | |

**Table 4**
First-order heat loss coefficient of PVT collectors with different combinations of glazing cavity filling (top row) and emissivity (left column).

| Heat loss coefficient, $a_1$ ($Wm^{-2}K^{-1}$) | $\varepsilon = 0.9$ | $\varepsilon = 0.5$ | $\varepsilon = 0.15$ | ST collector (Evacuated, $\varepsilon = 0.1$) |
|---|---|---|---|---|
| Air | 5.7 | 5.0 | 4.1 | 2.2 |
| Argon | 5.2 | 4.3 | 2.8 | |
| Evacuated | 4.6 | 3.3 | 1.8 | |

$\eta_0$, $a_1$and $a_2$ are shown for the different collector types in Table 3, Table 4 and Table 5, respectively. In each table, the right hand column shows the corresponding value for the ST collector for comparison. The zero-loss efficiency is similar for all PVT collectors due to the assumption of equal optical efficiency. In the temperature range of interest, heat loss is best compared using the first-order heat loss coefficient in Table 4. This comparison shows clearly the value of implementing convective and radiative control together. Applying an $\varepsilon = 0.15$ low-e coating to an air-filled collector reduces the heat loss coefficient by just 20%, whereas applying the same coating to an evacuated collector reduces it by nearly 60%.

Fig. 5(b) shows the electrical performance of PVT collectors employing PV cells with $\beta = 0.4$ and 0.2%/K. It should be observed that the PV cells operate at a higher temperature than the fluid outlet, due to the internal thermal resistances in the collector (in all collectors studied, the PV cells were 1–3 °C hotter than the fluid outlet). This is accounted for when calculating the electrical efficiency (Guarracino et al., 2016). The electrical efficiency is therefore also dependent on the type

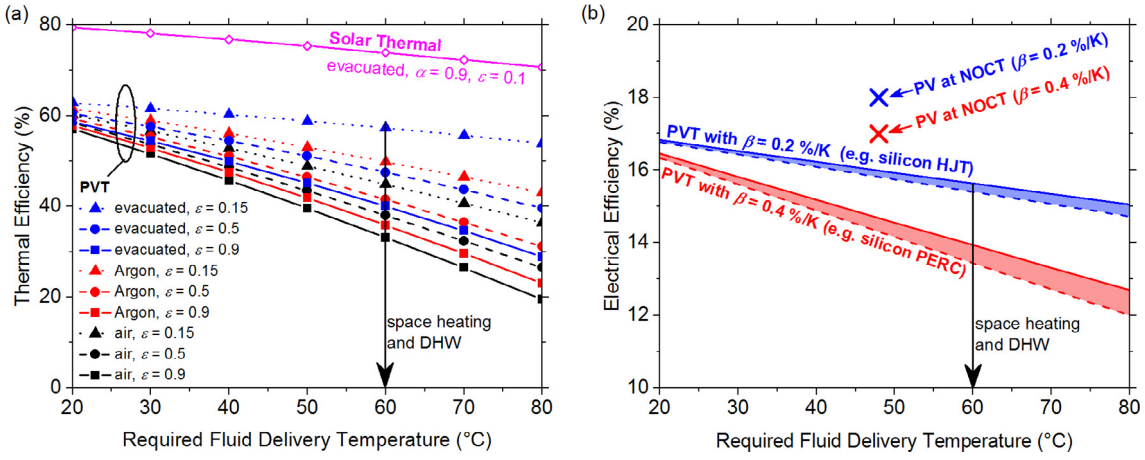


**Fig. 5.** Projected performance of different PVT collector designs as a function of the fluid delivery temperature. (a): The thermal efficiency of collectors employing different combinations of glazing cavities and low-e coatings, where the cavity filling and emissivity are given in the legend. Black, red and blue curves represent collectors with air, argon and evacuated cavities respectively. Solid curves with square markers represent ε = 0.9, dashed curves with circular markers represent ε = 0.5, and dotted curves with trangular markers represent ε = 0.15. (b): Electrical efficiency of PVT collectors employing PV cells with different temperature coefficients. For each PV cell type, there is a range of possible electrical efficiencies depending on the glazing cavity and low-e coating employed, and so a range is presented for each cell type, represented as a filled area bounded by solid and dashed curves. The crosses show the efficiency of purely PV panels employing the same cells types at NOCT.

**Table 5**
Second-order heat loss coefficient of PVT collectors with different combinations of glazing cavity filling (top row) and emissivity (left column).

| Heat loss coefficient, $a_2$ ($Wm^{-2}K^{-2}$) | $\varepsilon = 0.9$ | $\varepsilon = 0.5$ | $\varepsilon = 0.15$ | ST collector (Evacuated, $\varepsilon = 0.1$) |
|---|---|---|---|---|
| Air | 0.017 | 0.013 | 0.008 | 0.004 |
| Argon | 0.019 | 0.015 | 0.009 | |
| Evacuated | 0.018 | 0.013 | 0.005 | |

of thermal-loss control employed, since this affects the temperature difference between cell and fluid outlet. Fig. 5(b) therefore shows a coloured area for each cell type, representing the range of electrical efficiencies achieved over the range of collector types studied. Collector types with lower thermal loss have slightly lower electrical efficiency; however, this difference is significantly less than the difference between PV cell types.

Also shown for comparison are the NOCT efficiencies of PV modules based on the same PV cell types as the PVT collectors (blue and red crosses). It is interesting to compare these to the equivalent PVT collectors when delivering fluid at 60 °C. From the figure, a PVT collector operates three absolute percentage points lower than an equivalent PV module if both are based on PV cells with $\beta = 0.4\%/K$. This difference is due to additional optical losses in a glazed PVT collector, and the fact that the PV cell operate hotter in the PVT collector than in the PV module (at 60 °C fluid delivery temperature). However, this difference reduces to two absolute percentage points if both PVT and PV are based on PV cells with $\beta = 0.2\%/K$. This demonstrates the comparative advantage of using PV cells with low temperature coefficients when building PVT collectors for space heating and DHW.

In terms of absolute advantage, PVT collectors based on $\beta = 0.2\%/K$ cells perform two-percentage points higher than PVT collectors based on $\beta = 0.4\%/K$ cells when delivering 60 °C hot fluid. To put this improvement into context, the PV industry takes on average 6 years to improve the average PV module efficiency by two percentage points (Green, 2016); achieving a two-percentage-point improvement in PVT by swapping a one commercially-available cell type for another is therefore significant.

It has been shown in this section that PVT collectors employing convective and radiative control measures can better approach the thermal performance of ST collectors, and those based on low-temperature-coefficient PV cells can better approach the electrical performance of PV modules. However, when delivering a useful fluid temperature of 60 °C, even the best PVT collectors studied here deliver a lower thermal output than ST, and a lower electrical output than PV. Of course the benefit of the PVT collector is the combined electrical and thermal output. To properly compare PVT to PV and ST collectors, it is therefore necessary to develop a framework to compare electrical with thermal outputs and vice versa (Coventry and Lovegrove, 2003). This is performed in the following section.

## 5. Techno-economic analysis of future generations of PVT

For PVT technology to capture a significant portion of the energy market, it must demonstrate a reduced investment payback period compared to competing PV and ST technology. In this section, we assess how the performance improvements presented in the previous section are likely to affect the payback period of PVT collectors. The ultimate goal is identify the target costs at which PVT collectors must be sold and installed in order to compete with ST and PV, and to see how these may decrease as the technology develops along the roadmap.

To do this, we must estimate the comparative annual energy yields of the different types of collector, and make a quantitative comparison between the relative values of electrical and thermal energy, both in terms of dollar savings and carbon savings. As before, we focus on fluid delivery temperatures of 60 °C, since these are required to capture a significant fraction of global heat demand.

### 5.1. Annual energy yield

To compute the annual *electrical* energy yield, $Y_{el}$ (in $kWh_{el}m^{-2}year^{-1}$), PV and PVT systems, we use the simple relation

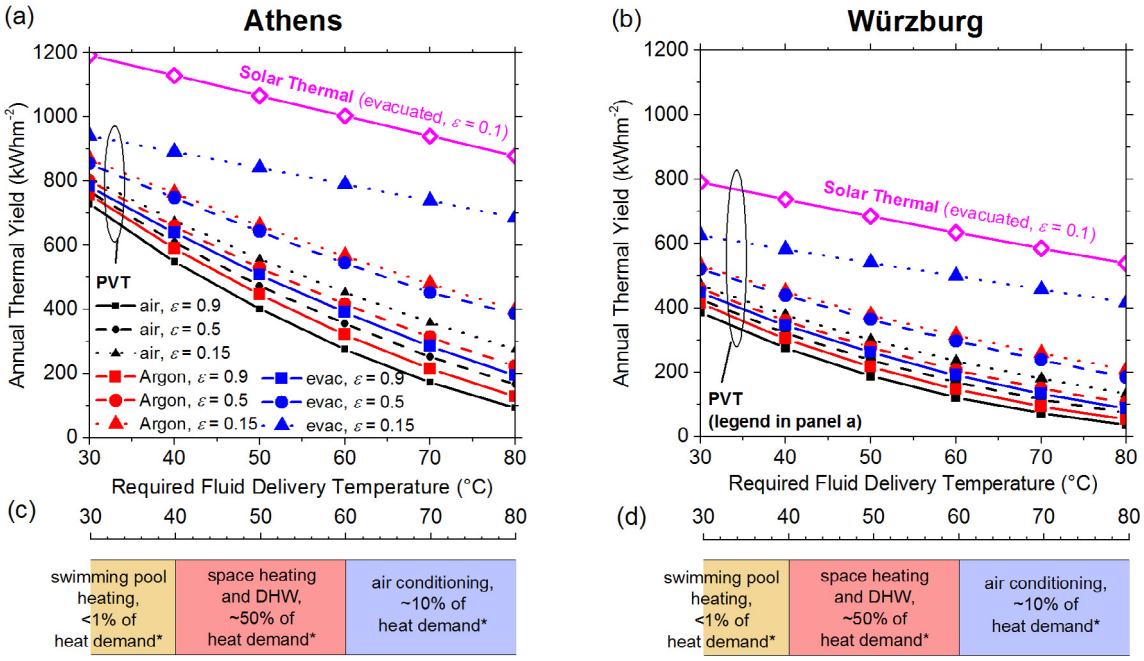


**Fig. 6.** The projected annual thermal yield of each collector in the roadmap, per unit of collector area, as a function of the fluid delivery temperature, for systems in Athens (a) and Würzburg (b). Shown for comparison are the same projections for a high-end solar thermal collector. These results are calculated using ScenoCalc (RISE, 2018) using the data in Tables 3–5, a panel title angle of 45°, an azimuthal rotation of 0°, and IAMs of 1 and 0.9 at 0 and 50° incidence, respectively. The annual insolation in Athens and Würzburg is H = 1781 kWh $m^{-2}$ and H = 1228 kWh $m^{-2}$, respectively.

$$Y_{el}^{PV} = PR_{el}\cdot H\cdot\eta_{el}^{PV}$$
$$Y_{el}^{PVT}(T_d) = PR_{el}\cdot H\cdot\eta_{el}^{PVT}(T_d) \quad (3)$$

where $H$ (kWhm$^{-2}$year$^{-1}$) is the annual insolation at the geographical location, and $PR$ (%) is the so-called performance ratio (PR). Following the usual definition of PR, the efficiency of PV panels, $\eta_{el}^{PV}$, used in Eqn. (3) is taken to be the rated efficiency under STC, i.e. at a cell temperature of 25 °C. The electrical efficiencies of the PVT panels, $\eta_{el}^{PVT}$, are taken as a function of the fluid delivery temperature following the simulation results in Section 4.

The PR accounts for all factors that cause the collector to yield less electrical power than that expected from the panel efficiency and local insolation. This includes soiling, shading, misorientation, downtime and power losses due to system components. A study of 100 German PV system installations found the annual $PR_{el}$ to vary between 70% and 90%, with an average of 84%(Reich et al., 2012). We therefore use $PR_{el}$ = 84% when calculating all PV and PVT annual yields in this work. The PR may vary geographically due to factors such as ambient temperature variation and local installation quality; however, there is no systematic reason why the $PR_{el}$ should change between the different collectors studied in this work, and so a constant $PR_{el}$ is considered appropriate for a comparative study.

The annual thermal energy yield, $Y_{th}$ (in kWh$_{th}$m$^{-2}$year$^{-1}$), of PVT and ST systems must be treated more carefully. Collectors with high heat loss will suffer particularly low yields at low light levels and low ambient temperatures, and so it is not appropriate to assume a constant $PR_{th}$ for all collectors. Instead, the annual thermal energy yield of the PVT and ST collectors studied in this work were calculated using the publically available calculation tool ScenoCalc (v5.01) (RISE, 2018) in steady-state mode. ScenoCalc calculates annual yield for a thermal collector using historical time-resolved weather conditions of select locations. In this work, calculations were performed for systems located in Athens (37°59′02.3″N 23°43′40.1″E), and Würzburg (49°47′N 9°56′E) to provide examples of warmer and cooler climes. The annual insolation in Athens and Würzburg is H = 1781 kWhm$^{-2}$ and H = 1228 kWhm$^{-2}$, respectively; these values are also used when calculating the PV contribution in these locations.

The input parameters ScenoCalc for each PVT panel are the zero-loss efficiency, $\eta_0$, the first-order heat loss coefficient, $a_1$ (Wm$^{-2}$K$^{-1}$), and the second-order heat loss coefficients, $a_2$ (Wm$^{-2}$K$^{-1}$), shown previously in Table 3, Table 4 and Table 5. A panel title angle of 45° and an azimuthal rotation of 0° is assumed in all calculations. The incidence angle modifier (IAM) is calculated using the so-called $b_0$ function, as is appropriate for flat plate collectors (Thomas et al., 1982), and the IAM at 50° is taken to be 0.9. As in Section 4, the PVT collectors have all been simulated with the collector in MPP mode, as is appropriate for synchronous heat and electricity generation.

The predicted annual yields in Athens and Würzburg are shown in Fig. 6(a) and (b) respectively. It can be seen that taking the annual yield as a figure of merit augments the relative difference between the different collectors in the roadmap. For instance, considering a 60 °C delivery temperature, the *thermal efficiency* of the best-performing PVT collector is 1.7 times higher than the worst-performing PVT collector; however, the *annual thermal yield* of the best-performing PVT collector is 2.9 times higher than the worst-performing PVT collector when situated in Athens, and 4.2 times higher when situated in Würzburg. This strengthens the case or higher-performing PVT as recommended by this roadmap, particularly for locations with lower light levels.Fig. 8.

### 5.2. Annual revenue and energy savings

To compare the competitivity of solar collectors, we must compare the revenue each collector generates per year. The annual revenue, $AR$, generated per m$^2$ of collector area can be estimated from the annual energy yield as follows

$$AR^{PV} = p_{el}\cdot Y_{el}^{PV}$$
$$AR^{ST}(T_d) = p_{th}\cdot Y_{th}^{ST}(T_d)$$
$$AR^{PVT}(T_d) = p_{el}\cdot Y_{el}^{PVT}(T_d) + p_{th}\cdot Y_{th}^{PVT}(T_d) \quad (4)$$

where $p_{el}$, $p_{th}$ are respectively the price at which the electrical and thermal energy are sold, or the price of the energy they displace.

Solar electricity is typically partly self-consumed and partly sold to the utility. Self-consumed electricity offsets electricity otherwise purchased at the retail electricity price. The price obtained for solar electricity sold to the utility – the so-called feed-in tariff (FiT) – depends strongly on government policy and varies from country to country. Generous FiTs well above the retail electricity price are becoming a thing of the past. However, FiTs that are in line with retail electricity prices remain common. In the UK, for example, electricity generated by solar rooftop systems is effectively sold to the utility at retail price when both the FiT and export tariff are considered (UK-Govt). In this work, we consider a high self-consumption scenario, and so take $p_{el}$ to be the retail electricity price. We assume a value of $p_{el}$ = 0.13 $/kWh, corresponding to the retail price in the US residential sector in 2016 (eia, 2017a).

Thermal energy must typically be used on site, and so $p_{th}$ must represent the price of the displaced energy. Thermal energy for heating and DHW is typically generated using a gas boiler, an electrical immersion boiler, or a heat pump. We discount electrical immersion boilers as being an overly expensive means of generating heat and focus instead, on gas boilers and heat pumps as being the principle competition to solar heat. For a gas boiler $p_{th}$ is the retail gas price, $p_g$, divided by the fuel-to-heat efficiency of the boiler, $\eta_{th}^{F}$. Focusing again on the US domestic sector in 2016, we take $p_g$ = 0.04 $/kWh (eia, 2017c), and $\eta_{th}^{F}$ = 90%, corresponding to medium-to-high-efficiency boiler, which leads to $p_{th}$ = 0.044 $/kWh. For an electrical heat pump, the annual average $p_{th}$ is the retail electricity price divided by the seasonal performance factor (SPF) of the heat pump. The SPF depends on the type of heat pump, the ambient temperature over the curse of the year, and building's heating system. SPFs of 2–4 are considered typical. Taking $SPF$ = 3, we arrive at $p_{th}$ = 0.043 $/kWh, which is similar to the price for a gas boiler. We therefore take $p_{th}$ = 0.043 $/kWh as the representative value of solar heat displacing either gas burned in a boiler or electricity used in a heat pump. This implies the relative dollar value of electricity and heat has roughly a 3:1 ratio.

From an environmental perspective, we can also estimate the annual carbon savings, $CS$ (kgCO$_2$m$^{-2}$year$^{-1}$), for each collector type, per m$^2$ of collector area per year, as

$$CS = CI_{el}\cdot Y_{el} + CI_{th}\cdot Y_{th} \quad (5)$$

where $CI_{el}$ and $CI_{th}$ are the carbon intensities of the displaced electrical and thermal energy. The carbon intensity of grid electricity varies greatly between geographical locations; for this simple analysis, we take the 2013 global average of $CI_{el}$ = 0.52 kgCO$_2$/kWh$_{el}$ (Ang and Su, 2016). Regarding the displaced thermal energy, natural gas has a carbon intensity of 0.18 kgCO$_2$/kWh$_{th}$ (eia, 2017b), so considering a gas boiler with an efficiency of $\eta_{th}^{F}$ = 90% we arrive at $CI_{th}$ = 0.2 kgCO$_2$/kWh$_{th}$. Alternatively, considering a heat pump with a SPF of 3, we arrive at $CI_{th} = CI_{el}/3$ = 0.17 kgCO$_2$/kWh$_{th}$. For convenience, we take the latter value, which maintains a 3:1 ratio between the relative value of electricity and heat, and allows us to plot annual revenue and carbon abatement on the same scale, using the conversion factor

$$CS = AR\frac{CI_{el}}{p_{el}} = AR \times 4.3 \ \text{kgCO}_2 \ \$^{-1} \quad (6)$$

Table 6 shows a summary of the different parameters discussed so far.

In Fig. 6(a) and (b) we show the $AR$ (left scale) and $CS$ (right scale) of the PVT collectors on this roadmap as a function of their fluid delivery temperature, along with that of a high-performance ST collector for comparison. We show also a single data point for PV modules,

**Table 6**
Parameters used in the techno-economic analysis framework.

| Symbol | Description | Value | Unit | Source |
|---|---|---|---|---|
| $PR_{el}$ | Performance ratio for solar electricity | 84% | | (Reich et al., 2012) |
| $SPF$ | Seasonal performance factor of a typical heat pump | 3 | | estimate |
| $\eta_{th}^{FF}$ | Fuel-to-heat efficiency of gas boiler | 90% | | estimate |
| $p_{el}$ | price of displaced electrical energy | 0.12 | $/kWh | (eia, 2017a) |
| $p_{th}$ | price of displaced thermal energy | 0.044 | $/kWh | (eia, 2017c) |
| $CI_{el}$ | carbon intensity of displaced electrical energy | 0.52 | kgCO2/ $kWh_{el}$ | (Ang and Su, 2016) |
| $CI_{el}$ | carbon intensity of displaced thermal energy | 0.17 | kgCO2/ $kWh_{el}$ | (eia, 2017b) |

denoting their *AR* and *CS* at the nominal operating cell temperature of 48 °C. The horizontal line emanating from the PV data point is a guide to eye to show at what delivery temperatures PVT and ST collectors deliver better value per unit area compared to PV. For simplicity, this plot assumes HJT cells ($\beta$ = 0.2%/K) for both the PV module and the PVT collectors. To put the fluid delivery temperature into context, we repeat in Fig. 6(e) and (f) the temperature ranges of different thermal demands along with the percentage of U.S. heat demand they represent. This is described in Section 2. and is originally from Fox et al. (2011). Fig. 6(a) shows results for systems located in Athens and Fig. 6(b) for systems located in Würzburg.

Fig. 6(a) and (b) are most instructive from the point of view of applications in which available roof space is a constraining factor. In much of the developed world, new buildings are subject to increasingly stringent emissions codes, which may oblige or encourage them to generate much of the building's energy needs from renewable or low-carbon sources on-site. Rooftop solar is scalable and readily integrated into buildings, and is therefore an attractive energy source. However, the energy demand of most modern buildings exceeds what can be

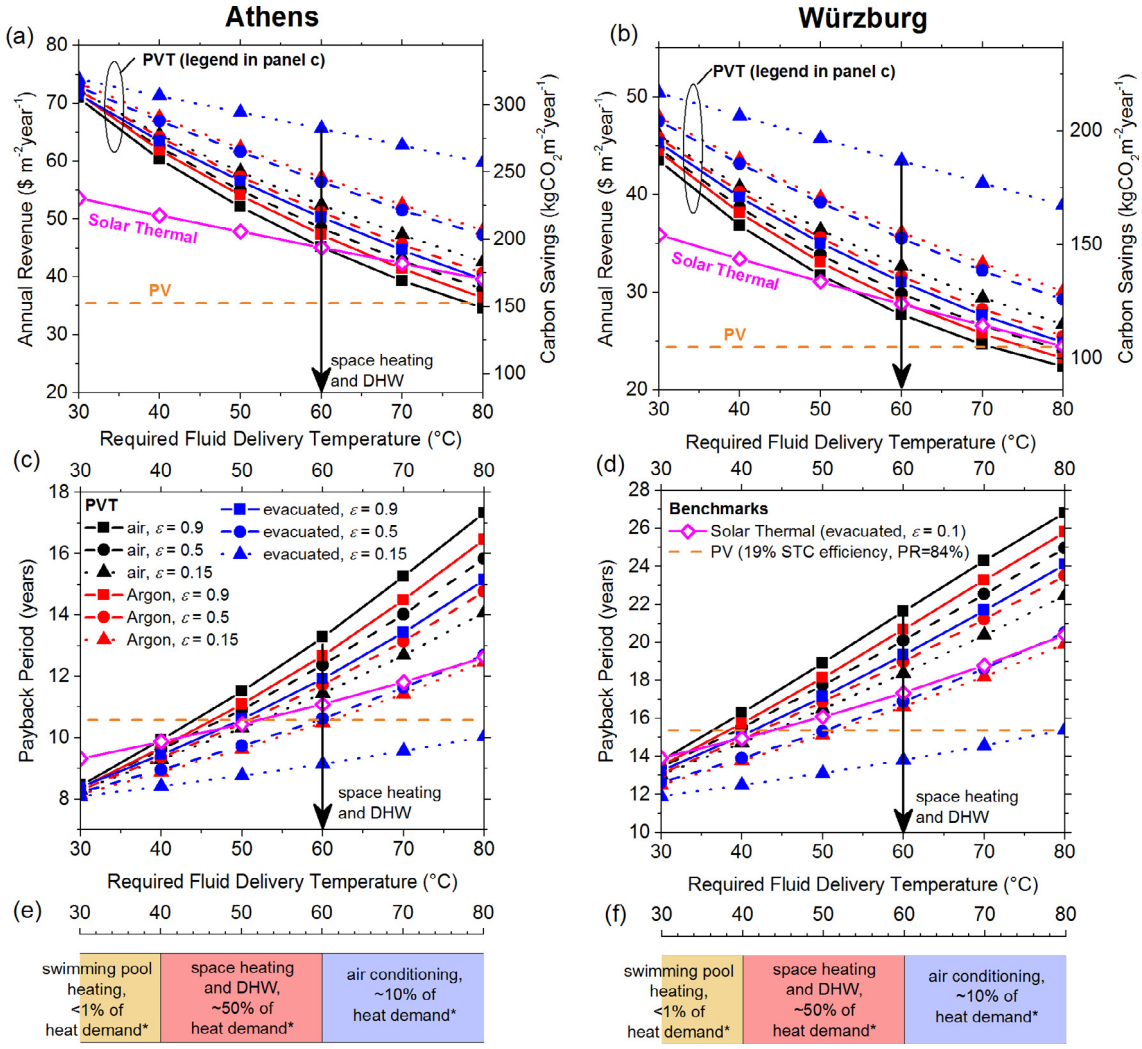


**Fig. 7.** (a) and (b): The projected annual revenue (left axis) and carbon savings (right axis) of each collector in the roadmap, per unit of collector area, as a function of the fluid delivery temperature, for systems in Athens (a) and Würzburg (b). Shown for comparison are the same projections for a high-end solar thermal collector, and for a silicon PV module with 19% taed efficiency at STC operating with an annually averaged performance ratio of 84%.Note that PV does not have a fluid delivery temperatyre, so a horizontal line is plotted for comparison. (c) and (d): The projected investment payback period for PVT, PV and ST systems, assuming exemplary system costs of $C_{PV}$ = 375 $ m$^{-2}$, $C_{ST}$ = 500 $ m$^{-2}$ and $C_{PVT}$ = 600 $ m$^{-2}$ , for systems in Athens (c) and Würzburg (d). (e) and (f): The temperature ranges of principle thermal demands along with the percentage of U.S. heat demand they represent. In (a) – (d), black, red and blue curves represent collectors with air, argon and evacuated cavities respectively; solid curves with square markers represent ε = 0.9, dashed curves with circular markers represent ε = 0.5, and dotted curves with trangular markers represent ε = 0.15.

generated by either solar PV or solar thermal over the building's footprint. The primary thermal demand in a building is for heating and DHW, and therefore a fluid delivery temperature of around $T_d = 60\,^{\circ}C$ would be required from a PVT or ST collector. It can be seen from Fig. 6 that for such a delivery temperature, the overall yield from the roof space, in terms of dollar or carbon savings, is maximised by installing PVT rather than just ST, PV or some combination side by side, even when considering the present generation of PVT collectors. Regarding the roadmap, it can be seen that a new generation of PVT collectors employing the loss control measures described here would fully maximise yield from a fixed roof space, achieving 1.5 and 2 times the revenue or carbon savings of PV modules and ST collectors, respectively, for the most advanced PVT collectors. The relative comparison between the different collectors is similar for Athens and for Würzburg (note the different scales), although the difference between collectors is more pronounced for Würzburg.

As discussed in the introduction, the results in Fig. 6(a) are likely to gain relevance – even outside the new-build sector – as increased solar penetration causes suitable roof space to become scare in urban areas. Based on an evaluation of available roof space, Hoogwijk and Graus have estimated the global technical potential of rooftop PV to be 40% of global electricity demand (Hoogwijk, 2004), and that of rooftop ST to be 70% of heat demand (Hoogwijk and Graus, 2008). Although these percentages seem large, the technical potential is a measure of the energy delivered if all suitable roof space is covered with PV or ST (exclusively in either case). It follows that rooftop scarcity in a high-penetration scenario is therefore likely. Although the market mechanism by which rooftop scarcity will translate to incentives for solar technologies with high-energy densities is so-far unclear, Fig. 6 suggests that PVT will become competitive in such a scenario.

### 5.3. Payback on investment

Where roof space is not the principle constraining factor, the true measure of competitivity that drives uptake is the so-called investment payback period, *PBP* (years). This is the length of time that the solar energy system has to operate before the owner has recuperated the cost of purchasing and installing the system. The simplest estimation of PBP is

$$PBP = C/AR \tag{7}$$

where $C$ is the cost of the fully installed system, per unit collector area.

The cost of solar installations can vary greatly as a function of geographical location, site, and technology (see International-Energy-Agency (2014) for PV, International-Energy-Agency (2012) for ST and Herrando and Markides (2016), Herrando et al. (2014) for PVT), and changes significantly over time. A cost-variable analysis is therefore performed in Section 5.4, along with a discussion of present system costs. However, as an illustrative example, we first present in Fig. 6(b)

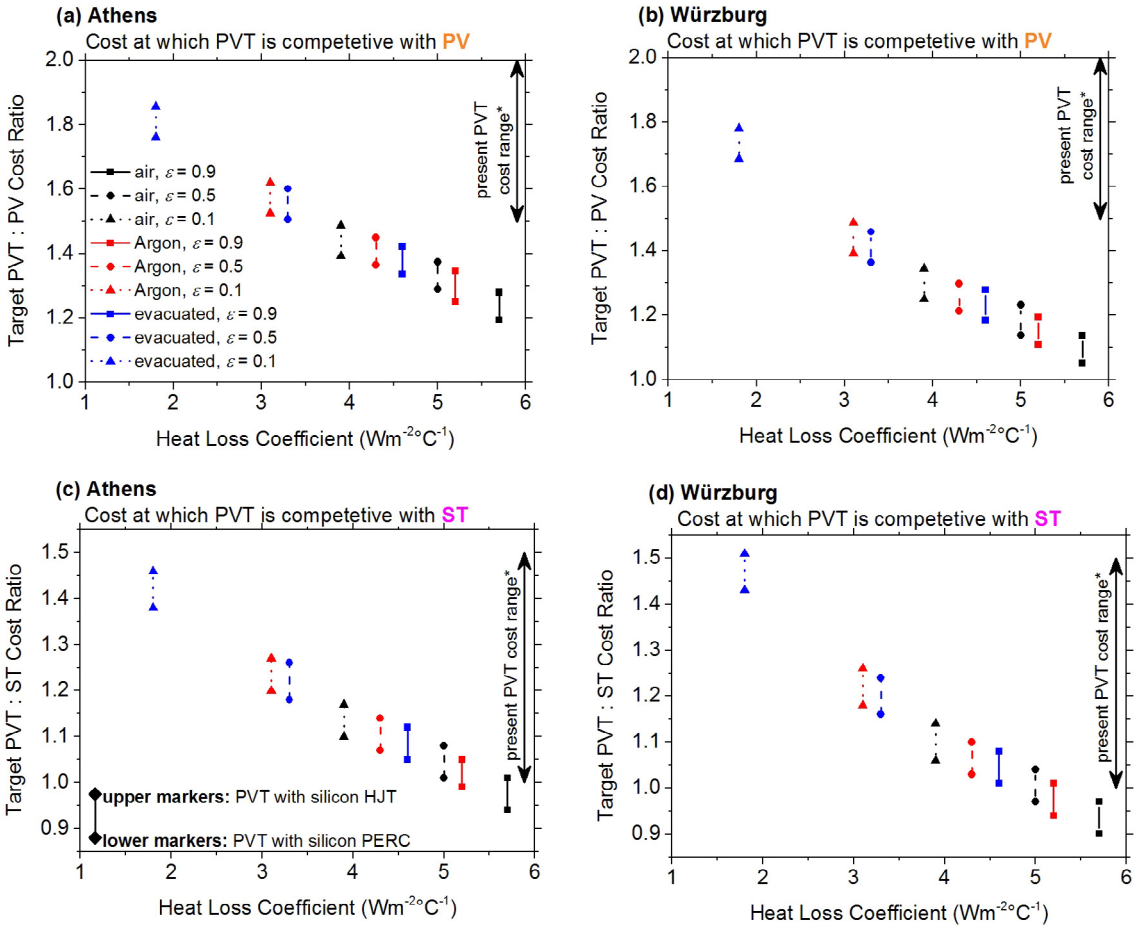


**Fig. 8.** The target cost at which the PVT systems based on the different collectors in the roadmap become competetive with PV and ST systems. The target cost is presented as a ratio between the PVT and PV (or ST) system cost, where all costs are of the fully installed system per unit of collector area. The x-axis shows the total heat loss coefficient of the PVT collector types, calculated in Section 3 (Table 4). The upper and lower markers are for PVT collectors employing silicon HJT and silicon PERC cells, respectively. The comparison is made for a fluid outlet temperature of 60 °C in the case of PVT and ST (PV systems are assumed to operate at NOCT = 48 °C). *The present PVT cost range is from a recent UK Government report (Strategy, 2016). (a): Comparison to PV in Athens. (b): Comparison to PV in Würzburg. (c): Comparison to ST in Athens. (d): Comparison to ST in Würzburg.

and (c) the payback period for PV, ST and PVT rooftop systems assuming exemplary costs of $C_{PV} = 375\,\$\,m^{-2}$, $C_{ST} = 500\,\$\,m^{-2}$ and $C_{PVT} = 600\,\$\,m^{-2}$. Fig. 6(a) shows results for systems located in Athens and Fig. 6(b) for systems located in Würzburg. Under this cost scenario, we see that the present generation of PVT (solid black curve, square markers) is only economically competitive with PV and ST systems for low-temperature applications such as swimming pool heating, whereas the more advanced collectors become competitive for the much larger space-heating and DHW market. The low-e evacuated collector even becomes competitive for sorption-based air-conditioning applications under this cost scenario. Again, the relative comparison between the different collectors is similar for Athens and for Würzburg (note the different scales), although the difference between collectors is more pronounced for Würzburg.

### 5.4. Target cost at which PVT becomes competitive

In reality, there is significant global-variability and uncertainty in the cost of solar installations. A 2016 NREL study reported the average cost of a fully installed PV rooftop system to be 2–3 $\$W^{-1}$ and the average rated power to be 160–170 $Wm^{-2}$(Fu et al., 2016); this implies a per unit area cost of $C_{PV} = 360–540\,\$\,m^{-2}$ for fully installed PV rooftop systems. ST systems have a far broader range of costs. In 2014, the IEA reported a global cost range of $200–1200\,\$\,m^{-2}$ for fully installed ST systems for DHW and space heating applications (Mauthner et al., 2014). This includes both flat-plate and evacuated-tube collectors; however, the broad range is due to geographical variation rather than variation between collector types.

PVT costs are less well documented, likely due to market immaturity. A 2016 UK Government report found the cost of installed PVT systems to be 1–1.5 times that of ST systems and 1.5–2 times that of PV systems (Strategy, 2016). However, given there is no consolidated PVT market in the UK, it is unclear if these prices will persist. Due to the uncertainty in PVT costs and the variability of ST costs, it is far more instructive to turn the analysis around and estimate the target costs at which PVT technology becomes competitive with the incumbent PV and ST technologies, i.e., the cost at which a fully installed PVT system will have the same investment payback period as a PV or ST system in the same location. This has been estimated for each collector type using the framework in Section 5.3. The comparison is made for a fluid outlet temperature of 60 °C in the case of PVT and ST (PV systems are assumed to operate at NOCT = 48 °C).

The target cost ratios are shown in Fig. 7, where the four graphs show comparisons to PV and to ST both in Athens and in Würzburg. The target cost is presented as a ratio between the PVT and PV (or ST) system cost, where all costs are of the fully installed system per unit of collector area. To further generalize the results, we show on the abscissa the total heat loss coefficient of the PVT collector types, calculated in Section 3 (Table 4). For each collector type, results are included for PVT collectors based on silicon PERC cells (lower markers) or silicon HJT cells (upper markers).

Fig. 7 is intended as a guide for researchers, technology developers and manufacturers to assess the costs that should be targeted for competitive PVT systems. Comparing target costs between PVT collectors also allows a cost-benefit analysis of prospective technology upgrades, once the increased cost incurred by the upgrade is known.

Fig. 7 also quantifies how the technology advancements detailed in Section 2 can relax the cost requirements of PVT collectors, and therefore increase their competitivity. The range of PVT system costs found in the aforementioned UK Government study (Strategy, 2016) are shown on the right axis of each plot. It can be seen that many of the collector types discussed in this work would become competitive if they were able to be delivered at similar prices to today's collectors. Of course adding low-e coatings, and gas-filled glazed cavities will increase the collector cost. However, given that the collector cost is typically less than half the cost of the installed system, it may be possible to implement these changes with minimal increase in overall cost, depending on the specific implementation.

## 6. Conclusions

A roadmap has been presented of the technological advances that are required for hybrid PVT solar collectors to realise their full potential in DHW and heating applications. Insulating cavities, low-emissivity coatings and PV cells with low temperature coefficients have been discussed as means of achieving high electrical and thermal efficiency at fluid delivery temperatures above 60 °C, and an ITO based transparent low-e coating applied directly to PV cells was presented for the first time. Simulations have been performed compare the performance of PVT collectors employing different combinations of these measures. Since PVT panels produce both electrical and thermal outputs, they cannot be compared on efficiency alone. Therefore, a formalism has been developed to compare PVT, PV and ST panels based on the carbon savings and financial payback they are expected to offer per unit collector area.

When the collector is delivering fluid at 60 °C, employing PV cells with low temperature coefficients, e.g. silicon HJT, is shown to add two percentage points to the electrical efficiency when compared to more standard Al-BSF or PERC cells. This is unlikely to motivate a switch to HJT at present prices, though this may change if the price gap between HJT and more standard cell types closes. Conversely, combining glazing cavities with low-emissivity coatings provides a much clearer route to improved performance and competitivity.

The most advanced PVT collector along the roadmap employs an evacuated glazing cavity combined with a low-e coating with an emissivity of $\varepsilon = 0.15$. Compared to present commercial PVT, this collector is projected to have double the thermal efficiency, and to provide 1.5 and 2 times the revenue or carbon savings of PV modules and ST collectors, respectively. A promising intermediate solution is an Argon-filed cavity combined again with an $\varepsilon = 0.15$ low-e coating. Comparing again to commercial PVT, this collector exhibits a 70% improvement in thermal efficiency and a 20% improvement in carbon savings and financial payback per meter squared. A gas-filled cavity is likely to be produced more cheaply than an evacuated cavity, and so this solution may also prove attractive.

An important argument for advancing PVT along the roadmap is that the improved performance allows PVT to become competitive at less demanding production, system and installation costs, which are typically larger than for equivalent PV and ST systems. It is estimated that a PVT system based on present commercial state-of-the-art collectors (air-filled glazing cavity, no low-e coating) must have a cost no greater than 1.2 times that of an area-equivalent PV system, and no greater than 1 times that of an area-equivalent ST system. This is a demanding requirement at today's PVT-system costs, particularly when comparing to rooftop PV, which dominates the rooftop solar market. However, for evacuated low-e PVT, this cost margin increases to nearly 2 times when comparing with PV, and nearly 1.5 times when comparing with ST. This is more realistic at today's costs, but must be judged against the additional cost of employing these measures, which is not explored here.

## Acknowledgements

This work was funded by the Engineering And Physical Science Research Council (EPSRC) grants High Temperature, High Efficiency PV-Thermal Solar System (EP/M025012/1) and Joint UK-India Clean Energy Centre (JUICE) (EP/P003605/1). A. Mellor was supported by the European Commission through Marie Sklodowska Curie International Fellowship, Grant No. DLV-657359.

## References


Al-Shamani, A.N., Yazdi, M.H., Alghoul, M.A., Abed, A.M., Ruslan, M.H., Mat, S., Sopian, K., 2014. Nanofluids for improved efficiency in cooling solar collectors – a review. Renew. Sustain. Energy Rev. 38 (Suppl. C), 348–367.

Alonso-Álvarez, D., Ferre Llin, L., Mellor, A., Paul, D.J., Ekins-Daukes, N.J., 2017a. ITO and AZO films for low emissivity coatings in hybrid photovoltaic-thermal applications. Sol Energy 155, 82–92.

Alonso-Álvarez, D., Llin, L.F., Mellor, A., Paul, D.J., Ekins-Daukes, N.J., 2017b. Comparative study of annealed and high temperature grown ITO and AZO films for solar energy applications. MRS Adv. 1–6.

Ang, B.W., Su, B., 2016. Carbon emission intensity in electricity production: a global analysis. Energy Pol. 94 (Suppl. C), 56–63.

Antonanzas, J., del Amo, A., Martinez-Gracia, A., Bayod-Rujula, A.A., Antonanzas-Torres, F., 2015. Towards the optimization of convective losses in photovoltaic–thermal panels. Sol Energy 116, 323–336.

Bisen, A., Das, P.P., Jain, R., 2011. Parametric studies of top loss coefficient of double glazed flat plate solar collector. MIt Int. J. Mech. Eng. 1 (2), 71–78.

Bloomberg-New-Energy-Finance, 2015. New Energy Outlook 2015: Long-term Projections of the Global Energy Sector.

Branz, H.M., Regan, W., Gerst, K.J., Borak, J.B., Santori, E.A., 2015. Hybrid solar converters for maximum exergy and inexpensive dispatchable electricity. Energy Environ. Sci. 8 (11), 3083–3091.

Buchberg, H., Catton, I., Edwards, D.K., 1976. Natural convection in enclosed spaces—a review of application to solar energy collection. J. Heat Transf. 98 (2), 182–188.

Cathro, K.J.C., E.A, Reid, A.F, 1975. Nickel black as Selective Absorbing Surface, in: Meeting on Appl. of Sol. Energy Res. and Dev. Melbourne, Australia.

Chen, S.H.P., Saxena, S.C., 1975. Thermal conductivity of argon in the temperature range 350 to 2500 K. Mol. Phys. 29 (2), 455–466.

Coventry, J.S., Lovegrove, K., 2003. Development of an approach to compare the 'value' of electrical and thermal output from a domestic PV/thermal system. Sol. Energy 75 (1), 63–72.

CSUN, 2017. PERC CSUN-S156-5BB. http://www.csun-solar.com/fileadmin/dateiablage/media/datasheets/m-cells/PERC-5BB_datasheet_____.pdf (accessed 13-11-2017).

Dupré, O., Vaillon, R., Green, M.A., 2015. Physics of the temperature coefficients of solar cells. Sol. Energy Mater. Sol. Cells. 140, 92–100.

eia, 2017. Average Price of Electricity to Ultimate Customers by End-Use Sector. https://www.eia.gov/electricity/monthly/epm_table_grapher.cfm?t=epmt_5_6_a (accessed 02-05-2017.

eia, 2017b. How much carbon dioxide is produced when different fuels are burned? https://www.eia.gov/tools/faqs/faq.php?id=73&t=11 (accessed 22-11-2017).

eia, 2017c. U.S. Prince of Natural Gas Delivered to Residential Consumers. https://www.eia.gov/dnav/ng/hist/n3010us3m.htm. (accessed 02-05-2017).

ENERGIES-SOL, 2015. Ficha tecnica PV-T. www.energies-sol.com/Files/45_ficha_tecnica_pvt.pdf (accessed 28 October 2016).

Eurofins, VOLTHER® POWERTHERM test report.

Fox, D.B., Sutter, D., Tester, J.W., 2011. The thermal spectrum of low-temperature energy use in the United States. Energy Environ. Sci. 4 (10), 3731–3740.

Fu, R., Chung, D., Lowder, T., Feldman, D., Ardani, K., Margolis, R., 2016. U.S. Solar Photovoltaic System Cost Benchmark: Q1 2016, in: NREL (Ed.). NREL.

Good, C., Chen, J., Dai, Y., Hestnes, A.G., 2015. Hybrid photovoltaic-thermal systems in buildings – a review. Energy Procedia 70, 683–690.

Green, M.A., 2016. Commercial progress and challenges for photovoltaics. Nat. Energy 1 (1), 15015.

Guarracino, I., Mellor, A., Ekins-Daukes, N.J., Markides, C.N., 2016. Dynamic coupled thermal-and-electrical modelling of sheet-and-tube hybrid photovoltaic/thermal (PVT) collectors. Appl. Therm. Eng. 101, 778–795.

Hamberg, I., Granqvist, C.G., 1986. Evaporated Sn-doped $In_2O_3$ films: basic optical properties and applications to energy-efficient windows. J. Appl. Phys. 60 (11), R123–R160.

Henshall, P., Eames, P., 2014. Performance of Evacuated FlatPlate Solar Collectors Integrated with Thermal Energy Storage Systems, UK Energy Storage Conference. University of Warwick, UK.

Herrando, M., Markides, C.N., 2016. Hybrid PV and solar-thermal systems for domestic heat and power provision in the UK: techno-economic considerations. Appl. Energy 161, 512–532.

Herrando, M., Markides, C.N., Hellgardt, K., 2014. A UK-based assessment of hybrid PV and solar-thermal systems for domestic heating and power: system performance. Appl. Energy 122, 288–309.

Hoogwijk, M.M., 2004. On the Global and Regional Potential of Renewable Energy Sources. Utrecht University.

Hoogwijk, M.M., Graus, W., 2008. Global Potential of Renewable Energy Sources: A Literature Assessment. REN21 – Renewable Energy Policy Network for the 21st Century.

International-Energy-Agency, 2008. Overview of PV/Thermal Solar System Products and Projects, Task 35. International Energy Agency.

International-Energy-Agency, 2012. Technology Roadmap: Solar Heating and Cooling, in: Agency, I.E. (Ed.).

International-Energy-Agency, 2014. Technology Roadmap: Solar photovoltaic energy, in: Agency, I.E. (Ed.).

ITRPV, 2017. International Roadmap for Photovoltaic. ITRPV.

Lämmle, M., Kroyer, T., Fortuin, S., Wiese, M., Hermann, M., 2016. Development and modelling of highly-efficient PVT collectors with low-emissivity coatings. Sol. Energy 130, 161–173.

Magalhães, P.M.L.P., Martins, J.F.A., Joyce, A.L.M., 2016. Comparative analysis of overheating prevention and stagnation handling measures for photovoltaic-thermal (PV-T) systems. Energy Procedia 91, 346–355.

Mauthner, F., Weiss, W., Spork-Dur, M., 2014. Solar Heat Worldwide, Markets and Contribution to the Energy Supply 2014. International Energy Agency.

Mayer, J.N., Philipps, S., Hussein, N.S., Schlegl, T., Senkpiel, C., 2015. Current and Future Cost of Photovoltaics. Long-term Scenarios for Market Development, System Prices and LCOE of Utility-Scale PV Systems. Fraunhofer ISE.

McDonald, G.E., 1975. Spectral reflectance properties of black chrome for use as a solar selective coating. Sol. Energy 17 (2), 119–122.

Mellor, A., Guarracino, I., Llin, L.F., Riverola, A., Thoms, S., Paul, D.J., Markides, C.N., Chemisana, D., Maier, S., Ekins-Daukes, N., 2016. Specially designed solar cells for hybrid photovoltaic-thermal generators, in: Photovoltaic Specialist Conference (PVSC), 2016 IEEE 43nd. Portland Oregon.

Meyer-Burger, 2017. Heterojunction Technology. https://www.meyerburger.com/user_upload/dashboard_news_bundle/da4c7a0b7c33e8e21ccddace78c76513b12cc727.pdf (accessed 13-11-2017).

Mittag, M., 2017. Reliability of TPedge PV Modules Successfully Tested. Fraunhofer ISE.

Naked-Energy, Virtu. http://www.nakedenergy.co.uk/ (accessed August 2016 2016).

National-Institute-of-Standards-and-Technology, NIST Chemistry WebBook. http://webbook.nist.gov/cgi/inchi?ID=C7440371&Type=JANAFG&Table=on#JANAFG (accessed 13-11-2017 2017).

Network, S.K., 2015. Specific CEN Keymark Scheme Rules for Solar Thermal Products – Version 28. CEN Certification.

Philibert, C., 2006. Barriers to Technology Diffusion: The Case of Solar Thermal Technologies. International Energy Agency.

Philipps, S., Warmuth, W., 2017. Photovoltaics Report. Fraunhofer Institute for Solar Energy Systems, ISE.

Power, E., 2006. The European Heat Market. Euroheat & Power, Belgium.

Reich, N.H., Mueller, B., Armbruster, A., van Sark, W.G.J.H.M., Kiefer, K., Reise, C., 2012. Performance ratio revisited: is PR > 90% realistic? Prog. Photovoltaics: Res. Appl. 20 (6), 717–726.

REN21, 2016. Renewables 2016, Global Status Report, Key Findings. Renewable Energy Policy Network for the 21st Century.

RISE, ScenoCalc – A Program for Calculation of Annual Solar Collector Energy Output. https://www.sp.se/en/index/services/solar/ScenoCalc/Sidor/default.aspx (accessed 15 May 2018).

Riverola, A., Mellor, A., Alonso Alvarez, D., Ferre Llin, L., Guarracino, I., Markides, C.N., Paul, D.J., Chemisana, D., Ekins-Daukes, N., 2018. Mid-infrared emissivity of crystalline silicon solar cells. Sol. Energy Mater. Sol. Cells 174, 607–615.

Rocky-Mountain-Institute, CohnReznick-Think-Energy, HOMER-Energy, 2014. The Economics of Grid Defection. Rocky Mountain Institute.

Santbergen, R., van Zolingen, R.C., 2008. The absorption factor of crystalline silicon PV cells: a numerical and experimental study. Sol. Energy Mater. Sol. Cells 92 (4), 432–444.

Shah, V., Booream-Phelps, J., 2015. Solar Industry Market Research: Crossing the Chasm. Deutsche Bank.

Shah, V., Booream-Phelps, J., Min, S., 2014. Solar Industry Market Research: 2014 Outlook: Let the Second Gold Rush Begin. Deutsche Bank.

Solar-Rating-and-Certification-Corporation, 2007. Summary Of SRCC Certified Solar Collector and Water Heating System Ratings. http://web.archive.org/web/20070220142139/http://www.solar-rating.org/SUMMARY/Dirsum_20070201.pdf (accessed December 2016 2016).

Solieman, A., Aegerter, M.A., 2006. Modeling of optical and electrical properties of In2O3: Sn coatings made by various techniques. Thin Solid Films 502 (1–2), 205–211.

Solimpeks, 2017. Powertherm. http://www.solimpeks.com/product/volther-powerthern/ (accessed 13-11-2017 2017).

Solimpeks, 2016. Volther Datasheet. http://www.solimpeks.com/wp-content/uploads/2012/12/Volther-Datasheet.pdf (accessed 28 october 2016).

Strategy, D.-f.-B.-E.-.-I., 2016. Evidence Gathering – Low Carbon Heating Technologies – Hybrid Solar Photovoltaic Thermal Panels, in: Department for Business, E.I.S. (Ed.).

Thomas, W.C., Dawson, I.A.G., Waksman, D., Streed, E.R., 1982. Incident angle modifiers for flat-plate solar collectors: analysis of measurement and calculation procedures. J. Sol. Energy Eng. 104 (4), 349–357.

TVP-Solar, TVP Solar Technology (accessed 07-11-2017).

UK-Govt, Feed-in tariffs: get money for generating your own electricity. https://www.gov.uk/feed-in-tariffs (accessed 13-12-2017).

Vestlund, J., Dalenbäck, J.-O., Rönnelid, M., 2012. Thermal and mechanical performance of sealed, gas-filled, flat plate solar collectors. Sol. Energy 86 (1), 13–25.

Vestlund, J., Rönnelid, M., Dalenbäck, J.-O., 2009. Thermal performance of gas-filled flat plate solar collectors. Sol. Energy 83 (6), 896–904.

Wang, R.Z., Ge, T.S., Chen, C.J., Ma, Q., Xiong, Z.Q., 2009. Solar sorption cooling systems for residential applications: options and guidelines. Int. J. Refrig. 32 (4), 638–660.

Yingli-Solar, 2017. Panda 60 Cell Series 2. http://d9no22y7yqre8.cloudfront.net/assets/uploads/products/downloads/DS_PANDA60Cell-30b_40mm_EU_UK_201409_v03.pdf (accessed 13-11-2017).

Zhang, Q.C., Mills, D.R., 1992. Very low-emittance solar selective surfaces using new film structures. J. Appl. Phys. 72 (7), 3013–3021.

Zondag, H., Van Helden, W., 2002. Stagnation Temperature in PVT Collectors, PV in Europe. Rome.

Zondag, H.A., 2008. Flat-plate PV-Thermal collectors and systems: a review. Renew. Sustain. Energy Rev. 12 (4), 891–959.